scientific reports



OPEN Facile microwave synthesis of various-shaped magnetite/ reduced graphene oxide heterostructures and their magnetization properties

Abdallah F. Zedan^{1,2⊠}, Sherif Moussa² & M. Samy El-Shall²

Heterostructures of magnetite (Fe₃O₄) nanoparticles and reduced graphene oxide (RGO) sheets are very common composite materials for different applications such as catalysis, energy storage, and biomedicine. Developing methods for the facile control of the size and shape of both freestanding Fe₃O₄ nanoparticles and those anchored onto RGO sheets is in demand. Herein, we report on the rapid and facile microwave synthesis (MWS) of Fe₃O₄ nanoparticles and Fe₃O₄/RGO with various sizes and shapes using the oleylamine (OAm)/oleic acid (OAc) ligand pair. The solvothermal synthesis using microwave irradiation (MWI) resulted in the concurrent conversion of graphene oxide (GO) into RGO and the in-situ formation of various-shaped Fe₃O₄ on RGO sheets. Freestanding Fe₃O₄ nanoparticles of various shapes were prepared using MWS for comparison. The morphological, structural, and surface properties of the samples were studied using different characterization techniques. The magnetization properties of the prepared samples were determined using a vibrating sample magnetometer. Variousshaped standalone and RGO-supported Fe₃O₄ nanoparticles including nanospheres, nanocubes, and nanotriangles were synthesized via MWI at 1000 W for 20 min by changing the ratios of the iron precursor and the OAm/OAc ligand pair. Interestingly, the MWI using OAm/OAc ligand pair of a molar ratio of 3:4 resulted in the in-situ formation of large hexagonal Fe₃O₄/RGO. The X-ray diffraction (XRD) and X-ray photoelectron spectroscopy (XPS) results confirm the crystallinity and spinel structure of the prepared Fe₃O₄ samples and prove the concurrent conversion of GO into RGO with assemblies of Fe₃O₄ nanoparticles. The magnetization measurements further emphasized the role of size and shape in affecting the magnetic properties of Fe₃O₆ and Fe₃O₆/RGO heterostructures. The results identify the qualities of the prepared samples and prove the MWS as a facile one-pot method for the preparation of Fe₃O₄ and Fe₃O₄/RGO heterostructures.

Keywords Nanoparticles, Microwave Synthesis, Iron Oxide, Graphene, Composites, Magnetism

Graphene is a two-dimensional (2D) carbon material with carbon atoms packed in a hexagonal lattice forming an atom-thick basal plane¹. The oxidized derivative of graphene (graphene oxide, GO) is the most widely common starting precursor to fabricate graphene, conventionally known as reduced graphene oxide (RGO)². The oxygencontaining functional moieties (e.g. hydroxyl, epoxy, and carboxyl groups) present at basal planes and edges of the GO sheets permit GO to interact covalently and non-covalently with various compounds. Such interactions have permitted the synthesis and development of a plethora of new functional and composite nanomaterials with tailored properties and different applications^{3,4}. Given the colloidal stability of GO sheets in many solvents, the chemical reduction of the oxygen-containing functional groups can convert GO into reduced graphene oxide (RGO)². RGO exhibits intriguing features including 2D topology, large specific surface area, high mechanical strength, thermal stability, and graphitized basal plane^{4,5}. RGO-based composite materials have shown great success in widespread applications in various fields such as catalysis, energy storage, chemical sensing, biosensing, electronics, and environmental remediation⁶.

¹National Institute of Laser Enhanced Science, Cairo University, Giza 12613, Egypt. ²Department of Chemistry, Virginia Commonwealth University, Richmond, VA 23284, USA. [™]email: azedan@vcu.edu

The impressive interest in the ferrimagnetic Fe₃O₄ (magnetite) nanoparticles has revealed a significant role in the formation of several new ferrimagnetic composites 7.8. Although Fe₃O₄ is a widely used magnetic material with a half-metallic character and strong spin polarization at room temperature, it suffers from limited saturation magnetization9. Nevertheless, the control of the morphological and size properties of ferrimagnetic Fe₃O₄ could be accompanied by enhanced magnetization and saturation magnetization 10. Furthermore, the grafting of Fe₃O₄ onto carbon materials such as RGO could form functional composite materials with improved magnetic and other properties9. Owing to the qualities of Fe₃O₄/RGO magnetic nanocomposites, they have been longstanding of interest for application in diverse fields such as energy storage, magnetic fluids, electromagnetic coating materials, environmental remediation, magnetic separation, catalysis, and nanodevices^{11–14}. For example, Qi et. al. reported the development of a hybrid Fe_3O_4/RGO structure with improved performance for lithium storage¹⁵. Patel and co-workers described the efficient use of Fe₃O₄/RGO composite for enzyme immobilization application ¹⁶. Also, Wang et. al developed a porous hybrid structure of Fe₃O₄/RGO that caused higher activity for glucose sensing¹⁷. Li et. al.¹⁸, Saba et. al.¹⁹, and Chenchen et. al.²⁰ reported that Fe₃O₄/RGO hybrid structures could serve as efficient microwave absorption materials for electromagnetic interference shielding and military security applications. Similarly, Tayebi Pak et. al. reported the high microwave absorption performance of Fe₃O₄/ RGO composite powders prepared by the solution combustion method¹³. Pryadko and co-workers reported that a composite filler of Fe₃O₄/RGO enhanced the average fiber diameters, ductility, and mechanical strength of some reinforced hybrid scaffolds. In addition, the Fe₃O₄-RGO imparted high saturation magnetization to the scaffolds¹². Qi and co-workers reported the high sensitivity of the Fe₃O₄/RGO nanocomposite for the chemical sensing of chloramphenicol compounds²¹. Similarly, Niranjana et al. reported the efficient electrochemical sensing of ascorbic acid using a Fe₃O₄/RGO multi-layered structure²². Moreover, nanocomposites based on functional Fe₃O₄ and RGO sheets have been shown to express improved electrochemical performance for energy storage applications²³. Also, coupling Fe₃O₄ and RGO led to improved electrochemical behavior of the hybrid platform, as reported by Zhao et. al.⁵. Ran et. al. studied the activation of calcium peroxide by Fe₃O₄/RGO as a synergistic catalyst for the remediation of perchloroethylene in groundwater²⁴. Along this side, Pryadko and co-workers found that the magnetic Fe₃O₄/RGO nanocomposite was effective at the removal of heavy arsenic from water with excellent uptake²⁵. All these applications of Fe₃O₄/RGO have encouraged the continuous effort for the development of synthetic strategies to prepare RGO-supported Fe₃O₄ nanoparticles with various sizes and shapes and obtain desirable magnetization and nanocomposite properties²⁶.

A wide array of synthesis techniques has been developed including aerosol synthesis, laser pyrolysis, and solution phase synthesis such as co-precipitation, ultrasound irradiation, high-temperature thermal decomposition, hydrothermal, solvothermal, sol–gel, and microwave synthesis (MWS) methods 26,27 . MWS constitutes a powerful synthetic chemistry approach, yet in a simple and rapid fashion. The rapid and uniform heating leads to an instantaneous rise of temperature and heat energy transfer resulting in high effective reaction temperatures and fast nucleation and growth. MWS has been one of the most successful in producing nanostructures of controlled size, shape, and properties including Fe_3O_4 and $RGO.^{28}$ Although a variety of shapes of Fe_3O_4 have been recently reported, 27,29,30 it remains desirable to develop economic methods to control the shape of RGO-supported Fe_3O_4 (e.g. by using MWS chemistry and controlling the type or concertation of reactants or surfactants).

In this work, a rapid MWS method for the facile preparation of various-shaped freestanding Fe_3O_4 nanoparticles, RGO, and Fe_3O_4 /RGO heterostructures is demonstrated. The MWS method enabled the concurrent reduction of GO into RGO and the in-situ formation of various-shaped Fe_3O_4 nanoparticles on RGO sheets in a one-pot synthesis. Under appropriate microwave irradiation (MWI) conditions, Fe_3O_4 nanoparticles including nanospheres, nanocubes, nanotriangles, and hexagons were synthesized by varying the ratio of the ligand pair of oleylamine (OAm) and oleic acid (OAc). Further to the facile MWS of various-shaped Fe_3O_4 /RGO, magnetization properties of the synthesized Fe_3O_4 and Fe_3O_4 /RGO of different size and shapes were studied. The results identify the qualities of the prepared Fe_3O_4 and Fe_3O_4 /RGO heterostructures and prove the MWS as a facile one-pot method for the preparation and grafting of magnetic Fe_3O_4 onto RGO sheets.

Materials and methods Materials

Chemicals were used as received including natural graphite (\sim 200 mesh, 99.9%, Alfa Aesar), sulfuric acid ($\rm H_2SO_4$, certified ACS, Fisher Scientific), potassium permanganate (KMnO₄, analytical reagent, Mallinckrodt), hydrogen peroxide ($\rm H_2O_2$, 30%, KMG), Iron (III) acetylacetonate (Fe(acac)₃, Aldrich, 99.95%), oleic acid (OAc, Aldrich, tech 90%), oleylamine (OAm, Aldrich, tech), benzyl ether (BE, ACS 99.9%, Aldrich), and dimethyl sulfoxide (DMSO, ACS 99.9%, Alfa Aesar).

Preparation of graphene oxide (GO)

Graphene oxide (GO) was synthesized via the oxidative treatment of high-purity natural graphite following a previous report in the literature². In a typical synthesis, 6 g of KMnO₄ was added to a mixture of 2 g of graphite powder and 46 ml of $\rm H_2SO_4$ in an ice bath. The reaction mixture was stirred for 5 h while maintaining the temperature of the mixture at 30 \pm 5 °C. Afterwards, 5 ml of 30% $\rm H_2O_2$ and 280 ml of deionized water were added to the reaction mixture. Then, the obtained GO sheets were vacuum-filtered, repeatedly rinsed with water, and finally dried in air. Finally, an aqueous stock solution of GO nanosheets with a solution density of 0.2 mg/ml was prepared by using ultrasonication.

Microwave synthesis of Fe₃O₄ and Fe₃O₄/RGO Heterostructures

For the microwave synthesis (MWS) of various-shaped Fe_3O_4 nanoparticles, a mixture of 280 μ mol of iron (III) acetylacetonate ($Fe(acac)_3$ in 105 mmol benzyl ether was prepared by vigorous stirring/sonication until complete

dissolution. Then, specific volumes of the oleylamine (OAm)/ oleic acid (OAc) ligand pair were added to the mixture under continuous stirring. Afterward, the reaction mixture was transferred to a microwave oven and irradiated with a 15-s on/off cycle for 20 min at a microwave power of 1000 W translating to a reaction temperature of 280 °C. Upon completion, the reaction mixture was cooled down to room temperature. The products were separated using a centrifuge and washed with a hexane/ethanol mixture three times. The synthesis of Fe_3O_4 nanospheres, nanocubes, and nanotriangles was realized via the addition of 4.2 mmol, 4.2 mmol, and 2.1 mmol of OAm, compared to 11.2 mmol, 2.8 mmol, and 2.8 mmol of OAc, respectively.

For the MWS of different Fe_3O_4/RGO heterostructures, a similar mixture of 280 μ mol of $Fe(acac)_3$, 105 mmol benzyl ether, 4.2 mmol of OAm, and 5.6 mmol OAc was prepared by vigorous stirring/sonication. Then, a non-aqueous solution of GO in DMSO (1 mg/ml) was added to the above mixture. The temperature of the reaction mixture was brought to 280 °C by MWI at 1000 W for 20 min. The final products were separated using a centrifuge and washed multiple times with a hexane/ethanol mixture. Table S1 lists the microwave-synthesized Fe_3O_4 and Fe_3O_4/RGO heterostructures of different shapes and the corresponding ratios of the precursor and surfactant materials.

Characterization

The prepared samples were characterized by using), a transmission electron microscope (TEM), scanning electron microscope (SEM), X-ray diffraction (XRD), X-ray photoelectron spectroscopy (XPS), and magnetic characterization using a vibrating sample magnetometer (VSM). TEM images were acquired using a JEM-1230 electron microscope (Jeol, Japan) equipped with a Gatan UltraScan 4000SP 4K x 4K CCD camera and operated at 120 kV. Samples for TEM were prepared using Formvar carbon-coated copper grids (300-mesh, Ted Pella). SEM images were collected using a Quantum DS-130S dual-stage electron microscope. XRD measurements were carried out at room temperature by using an X'Pert Philips Materials Research diffractometer equipped with a Cu $K_{\alpha 1}$ radiation source. XPS measurements were performed using an Escalab 250 (Thermo Fisher Scientific) spectrometer equipped with an Al X-ray source. Magnetic measurements were performed using Versalab VSM (Quantum Design, USA).

Results and discussion

The Fe_3O_4 and Fe_3O_4 /RGO heterostructures of different shapes were synthesized from the $Fe(acac)_3$ by MWI in benzyl ether using the OAm/OAc ligand pair. The MWS of freestanding Fe_3O_4 nanoparticles was performed first to better understand the effect of experimental conditions on the size and shape of growing particles. Table S1 lists the microwave-synthesized Fe_3O_4 and Fe_3O_4 /RGO heterostructures of different shapes and the corresponding ratios of precursor and ligand pair (OAm/OAc) materials. Figure 1 displays the TEM images of different-shaped Fe_3O_4 nanoparticles including nanospheres, cubes, and triangles synthesized by MWI of a mixture of $Fe(acac)_3$ (28 mmol) and benzyl ether (105 mmol) for 20 min at 1000 W/ 280 °C using varying molar ratios of OAm/OAc ligand pair. As can be seen in Fig. 1a–d, the use of 4.2 mmol OAm, 3.2 mmol OAc, or 4.2 mmol OAm mixed with either 5.6 or 11.2 mmol OAc led to the formation of spherical Fe_3O_4 nanoparticles with different average sizes. The estimated average sizes of the spherical Fe_3O_4 nanoparticles obtained using the aforementioned OAm/OAc ratios

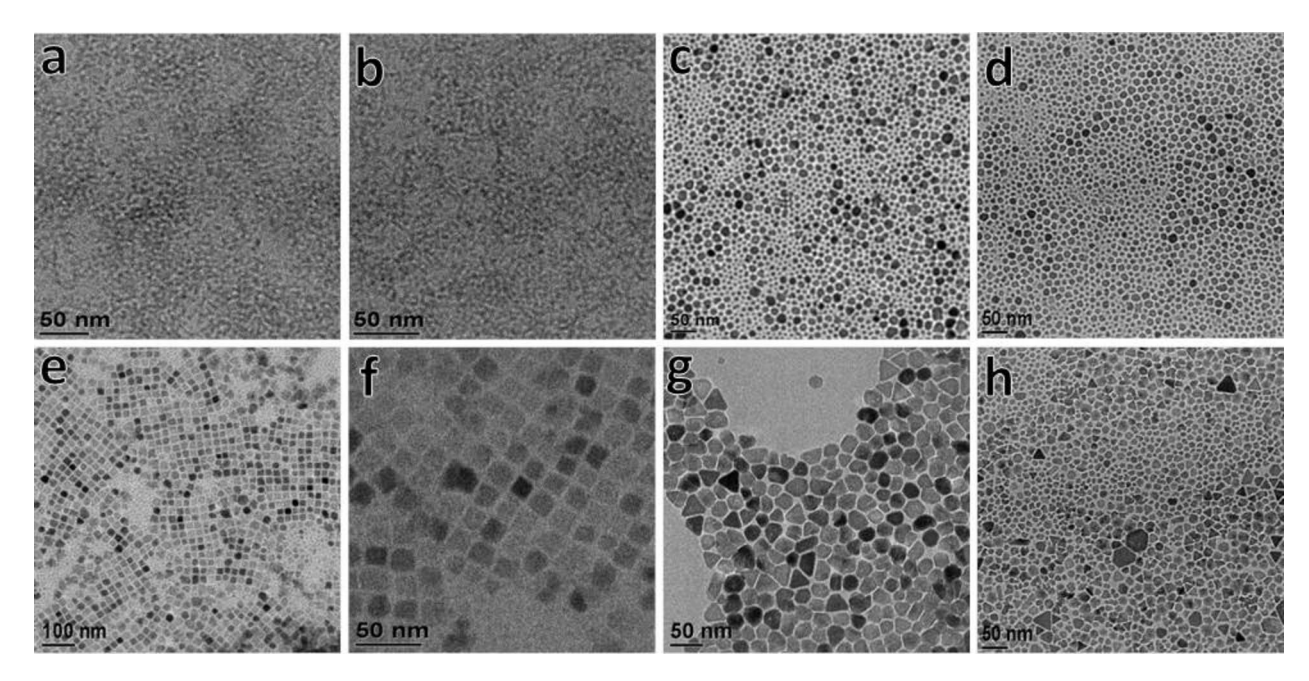


Fig. 1. TEM images of various-shaped Fe₃O₄ nanoparticles synthesized by MWI of a mixture of Fe(acac)₃ and benzyl ether for 20 min at 1000 W (280 °C) employing (a) 4.2 mmol OAc, (b) 3.2 mmol OAm), (c) 4.2 mmol OAm/ 5.6 mmol OAc, (d) 4.2 mmol OAm/ 11.2 mmol OAc, (e,f) 4.2 mmol OAm/ 2.8 mmol OAc, and (g-h) 2.1 OAm/ 2.8 mmol OAc.

are 3–4 nm (Fig. 1a), 4–5 nm (Fig. 1b), 10 ± 2 nm (Fig. 1c), and 13 ± 2 nm (Fig. 1d), respectively. The spherical Fe₃O₄ nanoparticles synthesized by MWI using OAm and OAc independently possess smaller sizes compared to those prepared using mixtures of OAm and OAc. This can be related to the relatively higher degree of surface passivation exerted by the self-assembly of the fatty chains of either OAm or OAc forming micellar structures. The micellar structures where Fe₃O₄ nuclei form could provide a further restriction on the growth of particles³¹. Also, the formation of smaller spheres using either OAm or OAc might be aided by the presence of benzyl ether favoring micellar formation. Interestingly, the interplay between the OAm and OAc was further employed to prepare Fe₃O₄ nanocubes and nanotriangles. When the relative concentration of OAc was decreased to 2.8 mmol while maintaining a 4.2 mmol OAm, well-defined Fe₃O₄ nanocubes of uniform size and shape with an average edge length of 15 ± 2 nm were obtained, as shown in Fig. 1e,f. On the other hand, maintaining the OAc fraction at 2.8 mmol while decreasing the OAm fraction to 2.1 mmol led to shape transformation into mostly Fe₃O₄ nanotriangles with 28 ± 2 nm edges and a few polyhedral nanoparticles, as can be seen in Fig. 1g,h. These TEM results suggest that the fine-tuning of the ratios of OAm and OAc co-surfactants can feasibly allow the microwave synthesis (MWS) of Fe₃O₄ nanoparticles with controllable size and shape under similar MWI conditions.

The MWS of various-shaped Fe₃O₄/RGO heterostructures was realized using a one-pot synthetic approach as described earlier³². For the MWS of Fe₃O₄/RGO, the aforementioned synthesis of freestanding Fe₃O₄ was adapted and combined with the feasible MWI-assisted approach for co-reduction of GO into RGO in DMSO described earlier³². Figure 2 and Figs. S1-S2 present the TEM and STEM images of freestanding RGO and spherical Fe₃O₄/ RGO heterostructures prepared by MWI of a mixture of Fe(acac)₃/benzyl ether and GO/DMSO at 1000 W for 20 min employing different ratios of the OAm and OAc co-surfactants. The TEM images of freestanding RGO prepared by MWI of GO in DMSO shown in Fig. 2a,b reveal the typical wrinkled topology of the 2D RGO sheets. As can be seen in the TEM images shown in Fig. 2c-f, a mixture of 4.2 mmol OAm and 5.6 mmol OAc led to the formation of spherical Fe₃O₄ with an average size of 10–13 nm supported on the RGO sheets. The STEM images shown in Fig. S1 further reveal the dispersion of the spherical Fe₃O₄ nanoparticles and the evident decoration of the RGO sheets. When the OAc fraction was further increased to 11.2 mmol, the in-situ formed Fe₃O₄ nanoparticles retained the spherical shape but slightly larger-sized particles were observed with an average size of 15-20 nm (Fig. S2). The MWI of a mixture of Fe(acac)₃/benzyl ether and OAm/OAc co-surfactants, in the presence of GO/DMSO, enabled the concurrent chemical reduction of GO into RGO and in-situ formation of spherical Fe₃O₄ nanoparticles on RGO sheets. Even though the RGO sheets are dense-decorated by spherical Fe₃O₄ nanoparticles, the TEM and STEM results still show uniform size, shape, and particle distribution (Figs. 2e,f, and S1).

Further, the effect of the relative concentrations of Fe- precursor, OAm, and OAc on the shape of Fe₃O₄ prepared in the presence of GO/DMSO was investigated. Figure 3 displays the TEM images of various-shaped Fe₃O₄/RGO heterostructures prepared by MWI of a mixture of Fe(acac)₃/benzyl ether and GO/DMSO at 1000 W for 20 min employing different ratios of Fe-precursor and co-surfactants. The MWI of a reaction mixture involving 0.28 mmol Fe, 2.1 mmol OAm, and 2.8 mmol OAc resulted in the formation of mostly triangle Fe₃O₄/RGO and

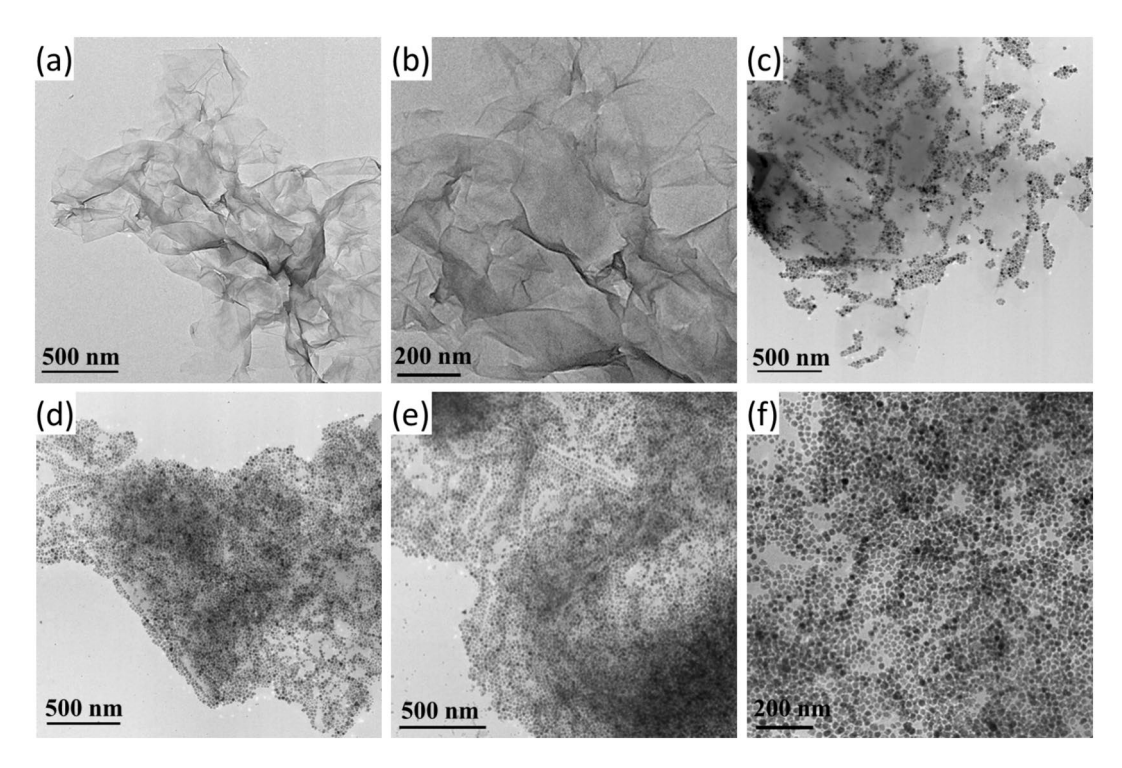


Fig. 2. TEM images of **(a,b)** freestanding RGO prepared by MWI of GO in DMSO, and **(c−f)** spherical Fe₃O₄/RGO heterostructures prepared by MWI of a mixture of Fe(acac)₃/benzyl ether and GO/DMSO at 1000 W (280 °C) for 20 min employing 4.2 mmol OAm and 5.6 mmol OAc.

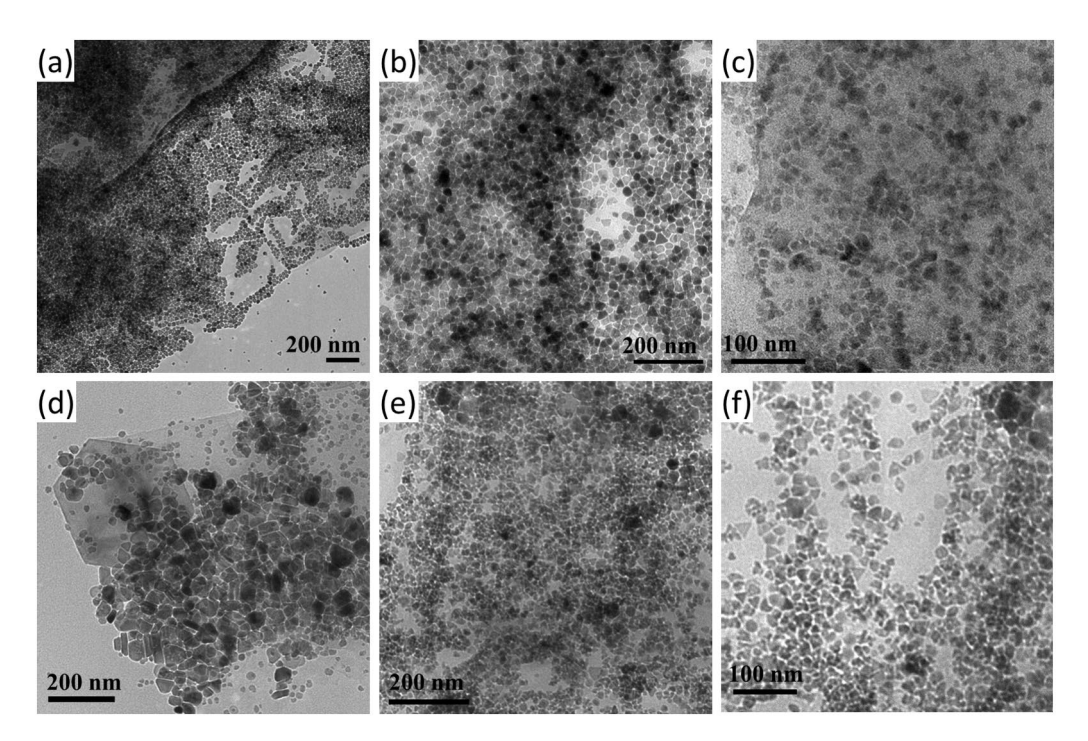


Fig. 3. TEM images of (**a,b**) triangle/hexagonal-, (**c**) cube-, (**d**) cube/hexagonal-, and (**e,f**) cube/triangle-shaped Fe₃O₄/RGO heterostructures prepared by MWI of a mixture of Fe(acac)₃/benzyl ether and GO/DMSO at 1000 W for 20 min employing different ratios of Fe-precursor and co-surfactants.

other small hexagonal particles (Fig. 3a,b). Upon increasing the OAm fraction to 4.2 mmol while keeping Fe and OAc the same, Fe₃O₄ cubes were formed on the surface of RGO sheets (Fig. 3c). An increase of the Fe from 0.28 mmol to 0.56 mmol while maintaining the OAm and OAc at 4.2 mmol and 2.8 mmol, respectively, led to the formation of a mixture of a cube and hexagonal Fe₃O₄/RGO sheets (Fig. 3-d) with average edge lengths of 28 ± 5 nm. Furthermore, the MWI of a mixture of 0.56 mmol, 2.1 mmol, and 5.6 mmol of Fe- precursor, OAm, and OAc, respectively, resulted in the formation of a mixture of cube and triangle Fe₃O₄/RGO sheets with average edge lengths of 9-11 nm (Fig. 3e,f). The TEM images shown in Fig. 3 mostly show good decoration of the 2D RGO sheets with various-shaped Fe₃O₄ nanoparticles including triangles, cubes, and hexagons, although mixtures of shapes and some irregular morphologies could also be observed. This suggests the presence of GO/ DMSO did not alter the feasibility of the MWS of various-shape Fe₃O₄ and findings similar to those in the absence of GO sheets could still be observed. Of particular interest, the MWS using OAm and OAc with a molar ratio of 0.75 in the presence of GO/DMSO resulted in the formation of large hexagonal Fe₃O₄ particles upon MWI at 1000 W for 20 min. The TEM and STEM images of the large hexagonal Fe₃O₄/RGO sheets are displayed in Figs. 4,5. The TEM images shown in Fig. 4 display large hexagonal Fe₃O₄ particles with an average edge length of ~ 0.9 μm that are formed on RGO sheets along with spherical Fe₃O₄ nanoparticles. The dark- and bright-field STEM images (Fig. 5) further reveal the wrapping of the hexagonal Fe₃O₄ by the RGO sheets decorated with small spherical Fe₃O₄ nanoparticles.

The above results indicate the power of coupling the ligand pair of OAm/OAc of a high-boiling point (≥350 °C) and the MWI for the controlled synthesis of diverse-shaped Fe₃O₄ and Fe₃O₄/RGO heterostructures. The MWI of a mixture of Fe(acac)₃ and OAm/OAc pair in a benzyl ether solvent can cause an instantaneous rise in temperature leading to the decomposition of the Fe(acac)₃ precursor, supersaturation, and burst of nucleation. During the MWI for 20 min, the nuclei further grow and Fe₃O₄ nanoparticles with isotropic or anisotropic shapes are formed due to the favorable growth provided by the preferential adsorption of the OAm/OAc ligand pair³³. Even though the linear molecular structures of the ligand pair of OAm (cisCH₃(CH₂)₇CH = CH)-(CH₂)₈NH₂) and OAc (cisCH₃(CH₂)₇CH = CH)-(CH₂)₇COOH) have nearly the same length for their alkyl chains, they possess different binding strengths or modes and exhibit distinct reducing abilities which have enabled the synthesis of metal and metal oxides of various anisotropic shapes³⁴. The OAm/OAc pair can serve as an efficient surface capping agent offering surface functionalization and anisotropic growth of nanoparticles³⁵. The rationale behind our facile preparation of Fe₃O₄ and Fe₃O₄/RGO heterostructures of controlled size and shape in benzyl ether solvent using MWI lies in the interplay of some physicochemical properties related to the OAm/OAc pair. For example, the different functional groups and binding abilities between OAm and OAc could result in the formation of diverse nanoparticle morphologies, depending on their relative molar ratios³⁴. The oxophilicity of OAc is higher than that of OAm, and thus OAc might have a stronger passivation effect by coordination with surface atoms of nanoparticles³⁶. The OAm might act as an activating agent for the decomposition of Fe(acac)₃ to Fe₃O₄ and not as a stabilizing agent since amine cannot efficiently stabilize Fe_3O_4 . The ratio of the OAm/OAc pair is known to influence the growth of Fe₃O₄ nanoparticles via terminating or slowing growth rate, for instance

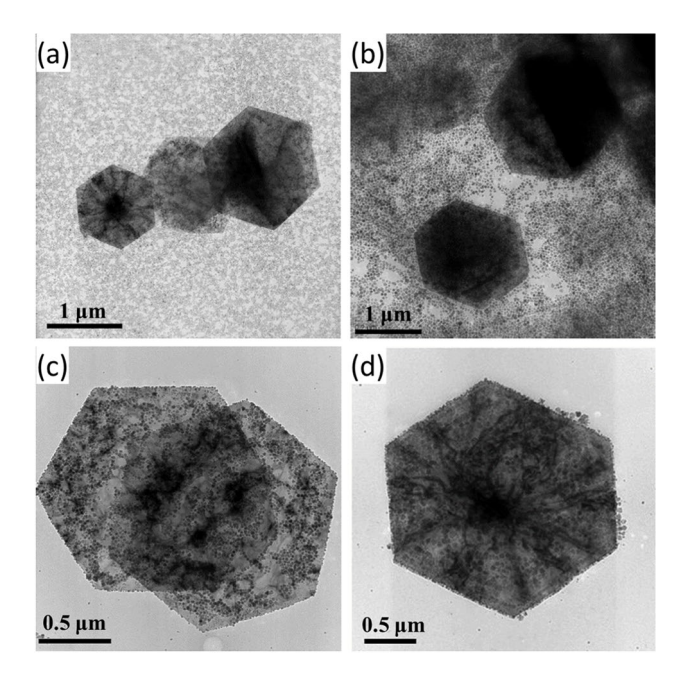


Fig. 4. TEM images of large hexagonal Fe_3O_4 formed along with the spherical Fe_3O_4/RGO by MWI of a reaction mixture of 0.28 mmol $Fe(acac)_3$, 4.2 mmol OAm, 5.6 mmol OAc in the presence of GO/DMSO at 1000 W for 20 min.

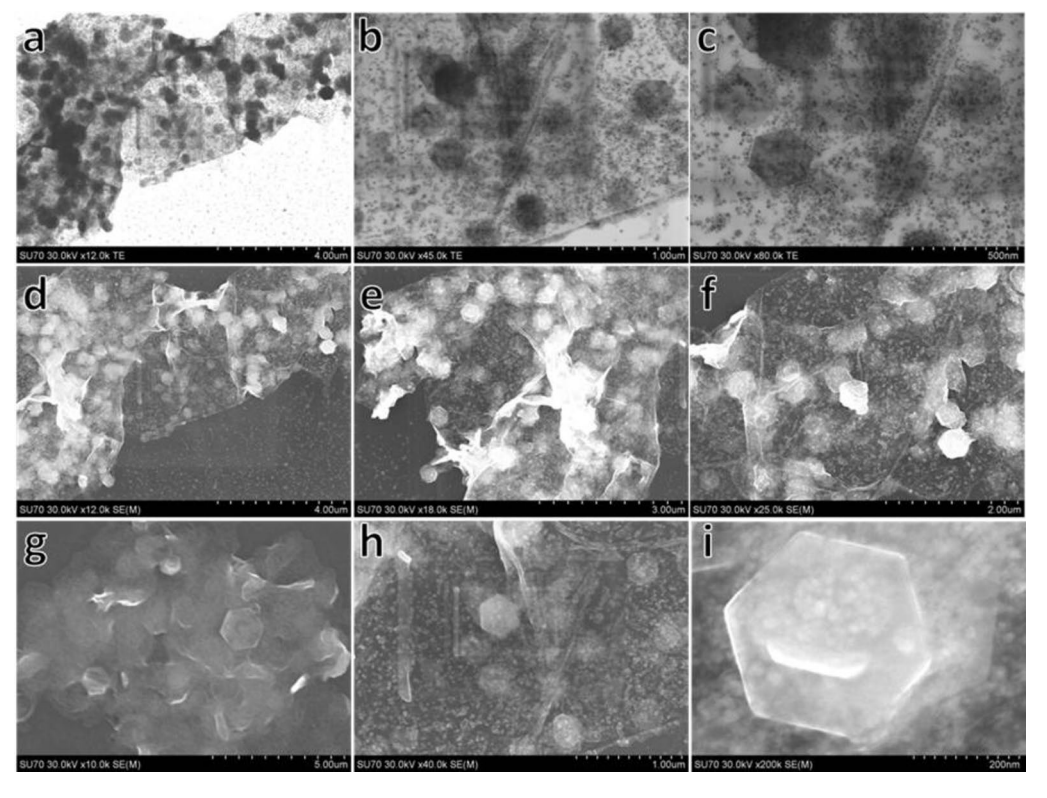


Fig. 5. (a–c) Dark-field and (d–i) bright-field STEM images of large hexagonal Fe_3O_4/RGO prepared by MWI of Fe-(acac) $_3/be$ nzyl ether in the presence of GO/DMSO at 1000 W for 20 min.

at the {100} facets. The favorable growth along the {111} facets with terminated {100} planes could break the growth symmetry and result in the formation of cube or triangle Fe₃O₄ nanoparticles³⁸. Because of the abundant oxygen-containing functional groups on the surface, GO is readily dispersed in DMSO and transformed into RGO upon MWI³². In the presence of GO/DMSO, the heterogeneous nucleation of Fe₃O₄ nanoparticles takes place concurrently with the in-situ chemical conversion of GO to RGO. The shape and size of the free-standing Fe₃O₄ and Fe₃O₄/RGO sheets depend on the experimental conditions that influence the degree of supersaturation, the nucleation rate, and the growth kinetics of the nanocrystal phase. For the MWS, these conditions include the decomposition rate of the Fe(acac)₃ precursor, the effective reaction temperature during the MWI process, the air oxidation process, the reaction time, and the rates of adsorption of the OAm/OAc ligand pair onto the nanoparticle surfaces. The relative binding energies of the OAm/OAc pair to the precursor molecules and the newly formed nanoparticles also affect the nucleation rate³⁹. In general, ligands that bind weakly to the precursors increase the nucleation rate while ligands that bind weakly to the newly formed nanocrystals enhance the growth rate. The competitive adsorption of OAm and OAc can effectively inhibit nanoparticle growth in all but the favorable crystallographic plane where the growth is significantly enhanced. The OAm binds on the surface of the ferrite nanoparticles weaker than OAc. A weakly binding ligand allows for further growth of the nanoparticles since the ligand can reversibly coordinate with the newly grown nanoparticles. This also allows for nanoparticle growth via the Ostwald ripening process where large nanoparticles grow even larger at the expense of smaller ones⁴⁰. In the absence or presence of GO, both OAm and OAc are thus essential for the control of the size, growth rate, and shape of the Fe₃O₄ nanoparticles.

The structural phase of selected Fe $_3$ O $_4$ and Fe $_3$ O $_4$ /RGO samples was confirmed using X-ray diffraction (XRD) measurements. Figure 6 shows the XRD patterns of spherical freestanding Fe $_3$ O $_4$, spherical Fe $_3$ O $_4$ /RGO, and hexagonal Fe $_3$ O $_4$ /RGO sheets prepared by MWI at 1000 W for 20 min using OAm/OAc ligand pair. The diffraction patterns of the three different samples are similar and match the profile of Fe $_3$ O $_4$ with an inverse cubic spinel structure (JCPDS: PDF No. 01–075-0449). The main XRD peaks centered around 30.1°, 35.5°, 38.2°, 43.2°, 53.66°, 57.1°, 62.7°, and 74.7° can be assigned to the (220), (311), (222), (400), (422), (511), (440), and (533) planes of spinel Fe $_3$ O $_4$. The selected area electron diffraction (SAED) diffraction patterns of spherical and hexagonal Fe $_3$ O $_4$ particles (Fig. S3) further confirm the crystallinity and characteristics of the spinel structure of Fe $_3$ O $_4$.

X-ray photoelectron spectroscopy (XPS) measurements were conducted to reveal the surface properties of selected Fe₃O₄ and Fe₃O₄/RGO samples prepared by MWS. Fig. S4 and Fig. 7 display the XPS profiles of lowresolution survey scans and high-resolution scan spectra of C 1s, O 1s, and Fe 2p elements for spherical Fe₃O₄, spherical Fe₃O₄/RGO, and hexagonal Fe₃O₄/RGO. The survey XPS scans (Fig. S4) show the prominent presence of the main elements of C, O, and Fe in the cases of both freestanding and RGO-supported Fe₃O₄ nanoparticles. The XPS peaks of indium (In 3d) originate from the indium foil used as a substrate for sample preparation. As outlined earlier, the solvothermal synthesis under MWI could lead to the concurrent conversion of GO into RGO and in-situ synthesis of Fe₃O₄ nanoparticles. The deconvoluted XPS peaks of C 1s (Fig. S4) show typical characteristics of carbon-containing bonding in both passivated Fe₃O₄ and Fe₃O₄/RGO. The main peak centered at about 284.8 in the cases spherical Fe₃O₄, spherical Fe₃O₄/RGO, and hexagonal Fe₃O₄/RGO is assigned to the C = C of the C 1s⁴³. The C 1s peaks observed higher binding energy in the cases of the three samples are attributed to the C-C and C-O bonding. The peak observed at 283.6 eV in the case of hexagonal Fe₃O₄/RGO can be assigned to the C-C bond as reported in a similar study⁴⁴. For the O 1s (Fig. S4), the deconvoluted XPS spectra show a main at around 530 eV and should peak at slightly higher binding energy. The XPS peak at 530 eV is attributed to the O 1s bonding of lattice oxygen species whereas the higher-binding energy peaks (531.4-531.8 eV) correspond to adsorbed oxygen species⁴⁵. The high-resolution XPS scans shown in Fig. 7 show typical XPS features of Fe 2p in the cases of spherical Fe₃O₄, spherical Fe₃O₄/RGO, and hexagonal Fe₃O₄/RGO. The main XPS peaks at around

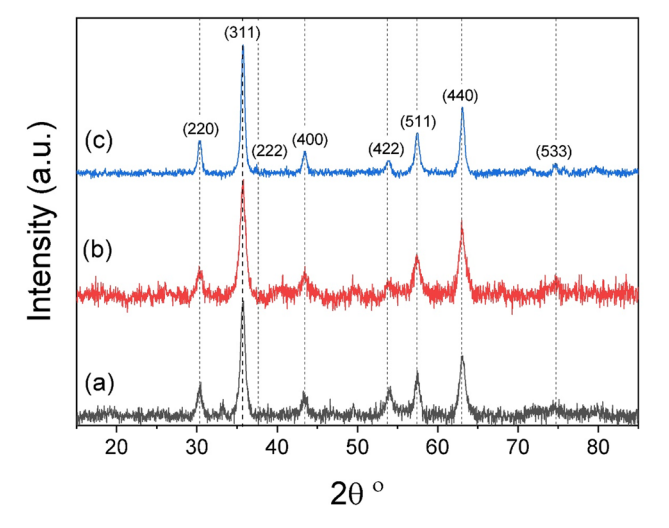


Fig. 6. XRD patterns of (a) spherical Fe₃O₄, (b) spherical Fe₃O₄/RGO, and (c) hexagonal Fe₃O₄/RGO sheets prepared by MWI at 1000 W for 20 min using OAm/OAc ligand pair.

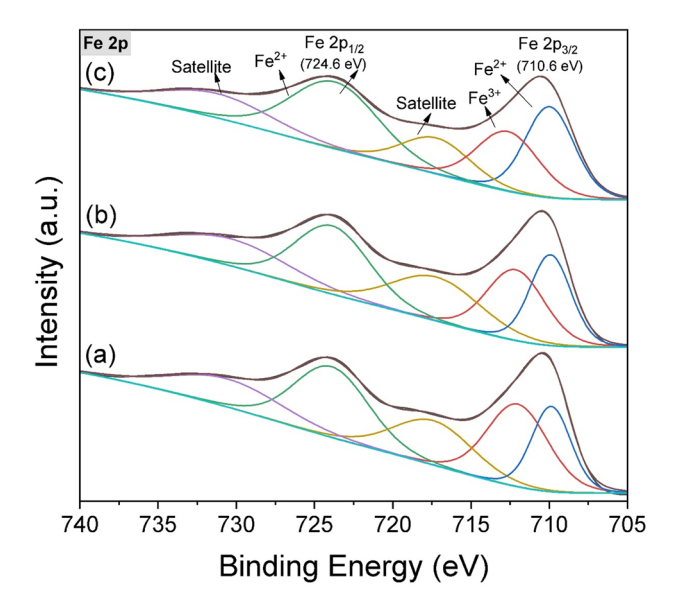


Fig. 7. High-resolution XPS spectra of Fe 2p for (a)spherical Fe_3O_4 , (b) spherical Fe_3O_4 /RGO, and (c) hexagonal Fe_3O_4 /RGO prepared by MWI at 1000 W for 20 min.

710.6 eV and 724.6 with a binding energy separation of 14 eV and their satellite peals are identical features of the Fe $2p_{3/2}$ and Fe $2p_{1/2}$ of Fe₃O₄ comprised of FeO (II) and Fe₂O₃ (III) subunits⁴⁶.

The magnetic properties of the prepared samples were studied by using vibrating sample magnetometer (VSM) measurements. The magnetic hysteresis of the microwave-synthesized freestanding Fe₃O₄ and Fe₃O₄/RGO heterostructures were recorded at room temperature. Figure 8 displays the hysteresis curves of different samples collected using an applied field in the range of – 30 to 30 kOe. The hysteresis loops of different samples reveal magnetic behavior with some superparamagnetic component at room temperature with nearly zero coercivity and low remnant magnetization values, as listed in Table S2. The low or zero remnant magnetization when the external magnetic field is removed matches the nearly superparamagnetic behavior reported for graphene sheets coated with Fe₃O₄ nanoparticles⁴⁷. The average size of the microwave-synthesized freestanding and RGO-supported Fe₃O₄ nanoparticles is less than the critical size of single domain particles, which is 54 nm for magnetite⁴⁸. This could result in distinct magnetic properties compared to bulk counterparts and the appearance of partial superparamagnetic components for the various-shaped Fe₃O₄. The shrinkage in size makes the magnetic anisotropic energy (KV), where K is the magnetic anisotropy constant and V is the volume of the particle, comparable to the thermal energy (kT), leading to randomization of magnetic moments and giving rise to some extent of superparamagnetism. It is generally accepted that the degree of saturation magnetization (M₈) increases with increasing size or crystallinity⁴⁸. Table S2 lists the magnitudes of saturation magnetization (M₈)

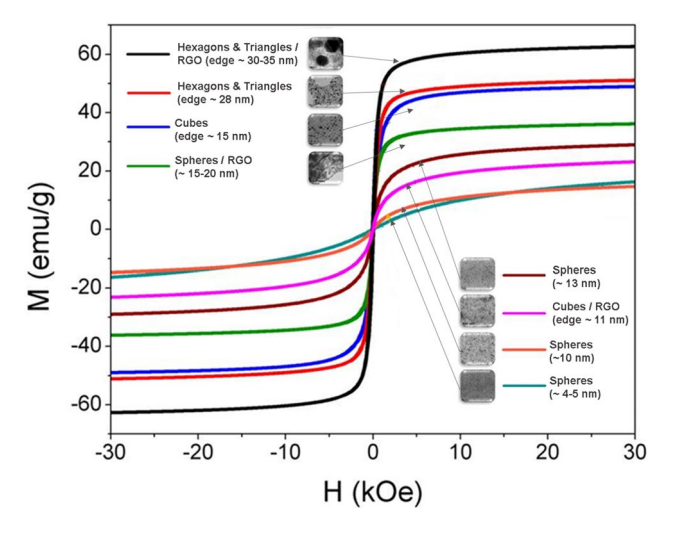


Fig. 8. Room-temperature hysteresis curves of various-shaped Fe_3O_4 and Fe_3O_4 /RGO heterostructures prepared by MWS at 1000 W for 20 min.

remnant magnetization (M_r) , and coercivity (H_r) for the various-shaped Fe₃O₄ and Fe₃O₄/RGO heterostructures. The microwaved synthesized samples show M_s values that are smaller than that of bulk magnetite grains (93 emu/g)⁴⁹. The decreased particle size, the increased surface defects, and the adsorption of surfactants onto the surface might result in structural disorders causing non-collinear spin structure, spin canting, and magnetic moment reduction⁴². The magnetization results shown in Table S2 and Fig. 7 indicate that with the change of the particle morphology from isotropic to anisotropic shape, generally the saturation magnetization increases, partly due to magnetocrystalline anisotropy-related factors 50. The change of the particles shape from spheres to triangles or cubes results in an increase in saturation magnetization to 62 emu/g for triangles and 51 emu/g for cubes, compared to 36 emu/g in case of spherical Fe₃O₄, in agreement with previous reports on hollow spheres, ⁴⁵ cubes, 42 octahedrons, 50 and hexapods 50 with M_s values of 56-65, 60.3, 72.5 and 96.2 emu/g, respectively. The freestanding triangle Fe₃O₄ nanoparticles possess saturation magnetization larger than that of triangle Fe₃O₄/ RGO sheets. Although magnitudes of M_s for spherical Fe₃O₄ and Fe₃O₄/RGO prepared by MWS are smaller than those of anisotropic-shaped Fe₃O₄, they still exhibit larger M_s higher than those reported for spherical magnetite (17.96 emu/g) and spherical magnetite supported on graphene (10.23 emu/g)⁵¹. The magnetization measurements show the effects of size and shape control on the magnetic properties of the microwave-synthesized Fe₃O₄ and Fe₃O₄/RGO heterostructures.

Conclusions.

Magnetite (Fe_3O_4) and Fe_3O_4 /RGO heterostructures are important nanocomposites for various catalysis, energy storage, and biological applications. Developing synthetic strategies for the rapid synthesis and feasible control of the size and shape of both freestanding Fe_3O_4 nanoparticles and those anchored onto RGO sheets is in demand. In this paper, a rapid and facile microwave synthesis (MWS) of Fe_3O_4 nanoparticles and Fe_3O_4 /RGO with various sizes and shapes using the oleylamine (OAm)/oleic acid (OAc) ligand pair is described. Freestanding Fe_3O_4 nanoparticles were also prepared using for comparison. The magnetization properties of the different prepared samples were investigated using vibrating sample magnetometry. Fe_3O_4 nanospheres, nanocubes, and nanotriangles were formed standalone and anchored onto RGO by employing various ratios of the iron precursor and OAm/OAc ligand pair under MWI. Interestingly, the in-situ formation of large hexagonal Fe_3O_4 /RGO was evident. The results confirm the crystallinity and spinel structure of the Fe_3O_4 samples and prove the simultaneous reduction of GO into RGO and grafting of Fe_3O_4 nanoparticles. Overall, the qualities of the prepared samples and the power of the MWS as a facile one-pot method for the preparation of Fe_3O_4 and Fe_3O_4 /RGO heterostructures are evident.

Data availability

We declare that all research data generated and/or analyzed during this study are included in the paper and its Supplementary Information file. Should any raw data files be needed in another format they are available from the corresponding author upon reasonable request.

Received: 19 June 2024; Accepted: 28 August 2024

Published online: 24 September 2024

References

- 1. Zedan, A. F. et al. Ultrasmall gold nanoparticles anchored to graphene and enhanced photothermal effects by laser irradiation of gold nanostructures in graphene oxide solutions. ACS Nano 7(1), 627–636 (2013).
- 2. Zedan, A. F., Moussa, S. & El-Shall, M. S. Rational synthesis of gold-ceria catalysts supported on reduced graphene oxide with remarkable activity for CO oxidation. *Mater. Res. Express* 10(2), 025007 (2023).
- 3. Mandal Goswami, M. Synthesis of Micelles Guided Magnetite (Fe3O4) Hollow Spheres and their application for AC Magnetic Field Responsive Drug Release. Sci. Rep. 6(1), 35721 (2016).
- 4. Iqbal, Z., Tanweer, M. S. & Alam, M. Reduced Graphene Oxide-Modified Spinel Cobalt Ferrite Nanocomposite: Synthesis, Characterization, and Its Superior Adsorption Performance for Dyes and Heavy Metals. ACS Omega 8(7), 6376–6390 (2023).
- 5. Zhao, P. et al. Tailored engineering of Fe3O4 and reduced graphene oxide coupled architecture to realize the full potential as electrode materials for lithium-ion batteries. J. Colloid Interf. Sci. 634, 737–746 (2023).
- Kavitha, C. A review on reduced Graphene oxide hybrid nano composites and their prominent applications. *Mater. Today Proc.* 49, 811–816 (2022).
- Bertolucci, E., et al. Chemical and magnetic properties characterization of magnetic nanoparticles. 2015 IEEE International Instrumentation and Measurement Technology Conference (I2MTC) Proceedings. (2015).
- 8. Mersal, M. et al. Fabrication of nitrogen doped TiO2/Fe2O3 nanostructures for photocatalytic oxidation of methanol based wastewater. Sci. Rep. 13(1), 4431 (2023).
- 9. Rashid, T. et al. Green Synthesis of Ni/Fe3O4/rGO Nanocomposites for Desulfurization of Fuel. ACS Appl. Nano Mater. 6(20), 18905–18917 (2023).
- 10. Chalasani, R. & Vasudevan, S. Form, Content, and Magnetism in Iron Oxide Nanocrystals. J. Phys. Chem. C 115(37), 18088–18093
- Jafari, F. & Rahsepar, F. R. V2O5–Fe3O4/rGO Ternary Nanocomposite with Dual Applications as a Dye Degradation Photocatalyst and OER Electrocatalyst. ACS Omega 8(38), 35427–35439 (2023).
- Pryadko, A. S. et al. Comprehensive Study on the Reinforcement of Electrospun PHB Scaffolds with Composite Magnetic Fe3O4– rGO Fillers: Structure, Physico-Mechanical Properties, and Piezoelectric Response. ACS Omega 7(45), 41392–41411 (2022).
- Tayebi Pak, A. et al. Hierarchical porous Fe3O4/RGO nanocomposite powders as high performance microwave absorbers. J. Market. Res. 13, 548–560 (2021).
- Sheikholia Lavasani, F. et al. Fabrication and characterization of the Fe3O4@SiO2-rGO nanocomposite: A catalyst for multicomponent reactions. Phys. Chem. Chem. Phys. 25(4), 2821–2829 (2023).
- 15. Qi, L. et al. Grape-Like Fe3O4 Agglomerates Grown on Graphene Nanosheets for Ultrafast and Stable Lithium Storage. ACS Appl. Mater. Interf. 8(27), 17245–17252 (2016).
- Patel, S. K. S. et al. Eco-Friendly Composite of Fe3O4-reduced graphene oxide particles for efficient enzyme immobilization. ACS Appl. Mater. Interf. 9(3), 2213–2222 (2017).

- 17. Wang, Q. et al. One-Pot Synthesis of Fe3O4 nanoparticle loaded 3D porous graphene nanocomposites with enhanced nanozyme activity for glucose detection. ACS Appl. Mater. Interf. https://doi.org/10.1021/acsami.6b16034 (2017).
- Li, W. et al. Facile synthesis of Fe3O4 nanoparticles/reduced graphene oxide sandwich composites for highly efficient microwave absorption. J. Coll. Interf. Sci. 645, 76–85 (2023).
- Ayub, S. et al. Optimization of magnetite with modified graphene for microwave absorption properties. J. Alloys Compounds 936, 168182 (2023).
- 20. Liu, C. et al. Straightforward modulation of graphene nanosheets with magnetic nanoclusters for ultrathin microwave absorption materials. Appl. Surf. Sci. 607, 154998 (2023).
- 21. Qi, X. et al. A simple one-step synthesis of Fe3O4/N-rGO nanocomposite for sensitive electrochemical detection of chloramphenical. Mater. Lett. 330, 133350 (2023).
- 22. Niranjana, J. S. et al. Novel synthesis of multi-layered rGO/Fe3O4 nanocomposite in a single step and its efficient electrochemical sensing of vitamin C. Mater. Sci. Eng. B 290, 116283 (2023).
- 23. Kalidass, J., Anandan, S. & Sivasankar, T. Rapid ultrasound driven self-assembled nanoarchitectonics iron oxide-reduced graphene oxide as an anode for Li-ion battery and its electrochemical performance studies. *J. Energy Storage* 74, 109361 (2023).
- 24. Xia, R., et al., Activation of calcium peroxide by graphene oxide-supported iron composite (Fe3O4/rGO) as a synergistic catalyst for perchloroethylene remediation. Research on Chemical Intermediates, 2023.
- 25. Han, R. et al. 1D Magnetic materials of Fe3O4 and Fe with high performance of microwave absorption fabricated by electrospinning method. Sci. Rep. 4(1), 7493 (2014).
- Fatima, H. et al. Shape-controlled synthesis of magnetic Fe3O4 nanoparticles with different iron precursors and capping agents. RSC Adv. 8(41), 22917–22923 (2018).
- 27. Qiao, L. et al. Standardizing size- and shape-controlled synthesis of monodisperse magnetite (Fe3O4) nanocrystals by identifying and exploiting effects of organic impurities. ACS Nano 11(6), 6370–6381 (2017).
- 28. Zedan, A. F. et al. Rapid synthesis of magnetic/luminescent (Fe 3 O 4/CdSe) nanocomposites by microwave irradiation. J. Nanoparticle Res. 15(1), 1312 (2013).
- Ranjan Sahu, S. et al. A facile synthesis of raspberry-shaped Fe3O4 nanoaggregate and its magnetic and lithium-ion storage properties. Mater. Sci. Eng. B 282, 115771 (2022).
- 30. Ba-Abbad, M. M. et al. Synthesis of Fe3O4 nanoparticles with different shapes through a co-precipitation method and their application. JOM J. Min. Metals Mater. Soc. 74(9), 3531–3539 (2022).
- 31. Wang, C. et al. A general strategy for synthesizing FePt nanowires and nanorods. Angewandte Chemie Int. Edition 46(33), 6333–6335 (2007).
- Zedan, A. F. et al. Ligand-controlled microwave synthesis of cubic and hexagonal CdSe nanocrystals supported on graphene. photoluminescence quenching by graphene. J. Phys. Chem. C https://doi.org/10.1021/jp107297x (2010).
- Manna, L., Scher, E. C. & Alivisatos, A. P. Synthesis of Soluble and Processable Rod-, Arrow-, Teardrop-, and Tetrapod-Shaped CdSe Nanocrystals. J. Am. Chem. Soc. 122(51), 12700–12706 (2000).
- 34. Mourdikoudis, S. *et al.* Oleic acid/oleylamine ligand pair: a versatile combination in the synthesis of colloidal nanoparticles. *Nanoscale Horizons* 7(9), 941–1015 (2022).
- Mohamed, M. B. et al. Growth Mechanism of Anisotropic Gold Nanocrystals via Microwave Synthesis: Formation of Dioleamide by Gold Nanocatalysis. ACS Nano 4(5), 2766–2772 (2010).
- 36. Si, R. et al. Rare-Earth Oxide Nanopolyhedra, Nanoplates, and Nanodisks. Angewandte Chemie International Edition 44(21),
- 3256–3260 (2005).
 37. Rajamathi, M., Ghosh, M. & Seshadri, R. Hydrolysis and amine-capping in a glycol solvent as a route to soluble maghemite gamma-
- Fe2O3 nanoparticles. Chem. Commun. 10, 1152–1153 (2002).
 38. Hees, J. et al. Nanocrystalline Diamond Nanoelectrode Arrays and Ensembles. ACS Nano https://doi.org/10.1021/nn2005409 (2011).
- 39. Abdelsayed, V. et al. Synthesis, passivation, and stabilization of nanoparticles, nanorods, and nanowires by microwave irradiation, in nanoparticles: synthesis, stabilization, passivation, and functionalization 2008. Am. Chem. Soc. https://doi.org/10.1021/bk-2008-0996.ch017 (2008).
- 40. Ratke, L. Voorhees, Growth and Coarsening Ostwald Ripening in Materials Processing 2002 (Springer-Verlag, 2002).
- 41. Zhuang, L. et al. Preparation and Characterization of Fe3O4 Particles with Novel Nanosheets Morphology and Magnetochromatic Property by a Modified Solvothermal Method. Sci. Rep. 5(1), 9320 (2015).
- 42. Gao, G. et al. Shape-Controlled Synthesis and Magnetic Properties of Monodisperse Fe3O4 Nanocubes. Crystal Growth Des. 10(7), 2888–2894 (2010).
- 43. Yang, X. et al. Nitrogen-doped Fe3C@C particles as an efficient heterogeneous photo-assisted Fenton catalyst. RSC Adv. 7(25), 15168–15175 (2017)
- 44. Bhaumik, A. *et al.* Reduced graphene oxide thin films with very large charge carrier mobility using pulsed laser deposition. *J. Mater. Sci. Eng.* **6**(4), 1–11 (2017).
- 45. Zedan, A. F. et al. Tailoring the reducibility and catalytic activity of CuO nanoparticles for low temperature CO oxidation. RSC Adv. 8(35), 19499–19511 (2018).
- Kong, F. et al. Magnetic properties and electrocatalytic properties of Fe5C2 particles with different morphologies. J. Mater. Sci. Mater. Electron. 33(2), 884–893 (2022).
- 47. He, H. & Gao, C. Supraparamagnetic, conductive, and processable multifunctional graphene nanosheets coated with high-density Fe3O4 nanoparticles. ACS Appl. Mater. Interf. 2(11), 3201–3210 (2010).
- 48. Xiong, Y. et al. Synthesis and assembly of magnetite nanocubes into flux-closure rings. J. Phys. Chem. C 111(19), 6998-7003 (2007).
- 49. Ye, Q.-L. et al. Effects of the unique shape of submicron magnetite hollow spheres on magnetic properties and domain states. Phys. Rev. B 75(22), 224404 (2007).
- Wang, X. et al. Shape-Control and Characterization of Magnetite Prepared via a One-Step Solvothermal Route. Crystal Growth Des. 10(7), 2863–2869 (2010).
- 51. Su, J. et al. Fe3O4–graphene nanocomposites with improved lithium storage and magnetism properties. J. Phys. Chem. C 115(30), 14469–14477 (2011).

Acknowledgements

We thank the National Science Foundation (CHE-1900094) for the support of this work. We thank Natalie Herring for her help with the SAED measurements.

Author contributions

A.F.Z. conducted the experiments, S.M. carried out some characterization, M.S.E supervised the project and managed the grant, A.F.Z. wrote the first draft, M.S.E. edited the manuscript. All authors reviewed the manuscript.

Competing interests

The authors declare no competing interests.

Additional information

Supplementary Information The online version contains supplementary material available at https://doi.org/10.1038/s41598-024-71537-6.

Correspondence and requests for materials should be addressed to A.F.Z.

Reprints and permissions information is available at www.nature.com/reprints.

Publisher's note Springer Nature remains neutral with regard to jurisdictional claims in published maps and institutional affiliations.

Open Access This article is licensed under a Creative Commons Attribution-NonCommercial-NoDerivatives 4.0 International License, which permits any non-commercial use, sharing, distribution and reproduction in any medium or format, as long as you give appropriate credit to the original author(s) and the source, provide a link to the Creative Commons licence, and indicate if you modified the licensed material. You do not have permission under this licence to share adapted material derived from this article or parts of it. The images or other third party material in this article are included in the article's Creative Commons licence, unless indicated otherwise in a credit line to the material. If material is not included in the article's Creative Commons licence and your intended use is not permitted by statutory regulation or exceeds the permitted use, you will need to obtain permission directly from the copyright holder. To view a copy of this licence, visit http://creativecommons.org/licenses/by-nc-nd/4.0/.

© The Author(s) 2024